Journal of Power Sources 222 (2013) 79–87

Contents lists available at SciVerse ScienceDirect

Journal of Power Sources

journal homepage: www.elsevier.com/locate/jpowsour

PtCu/C and Pt(Cu)/C catalysts: Synthesis, characterization and catalytic activity towards ethanol electrooxidation

Malika Ammam, E. Bradley Easton*

Faculty of Science, University of Ontario Institute of Technology, 2000 Simcoe Street North, Oshawa, ON L1H 7K4, Canada

HIGHLIGHTS

- ► PtCu/C and core–shell like Pt(Cu)/C catalysts were prepared.
- ► PtCu/C alloy catalysts have a Pt rich surface while core–shell like Pt(Cu)/C have a more Cu rich surface.
- ► PtCu/C alloy catalysts have greater activity towards ethanol oxidation than core–shell like Pt(Cu)/C catalysts.

ARTICLE INFO

Article history:
Received 29 June 2012
Received in revised form
26 July 2012
Accepted 31 July 2012
Available online 27 August 2012

Keywords:
Ethanol electrooxidation
Electrocatalysis
Binary alloys
Core shells based Pt and Cu

ABSTRACT

Binary catalysts containing Pt and Cu have been synthesized by two different methods. The first method consists of mixing Pt^{4+} and Cu^{2+} cations in presence of $NaBH_4$ to form PtCu/C alloy catalyst. In the second method, Cu/C nanoparticles were first synthetized then treated with Pt^{+4} in presence of $NaBH_4$ in an attempt to form core shells Cu covered by Pt, Pt(Cu)/C. The synthesized catalysts PtCu/C and Pt(Cu)/C were characterized by Inductively Plasma Emission Spectroscopy (ICP), Transmission Electron Microscopy (TEM), Thermogravimetric Analysis (TGA), X-ray diffraction (XRD), X-ray Photoelectron Spectroscopy (XPS), and Electrochemistry. XRD studies indicate that Pt–Cu alloy has formed in both cases even using the second synthetic method that is supposed to yield Cu covered by Pt core shells. The latter was attributed to the dissolution of Cu/C nanoparticles during their treatment with Pt^{4+}. This was confirmed by XRD and TEM where significant decrease in the grain size from ~37.2 nm obtained for Cu/C to ~3 nm for Pt(Cu)/C was observed. While ICP analysis revealed similar Pt and Cu contents in each catalyst, XPS showed that PtCu/C is Pt rich at the surface and Pt(Cu)/C is Cu rich at the surface of the nanoparticles. In turn, this surface segregation influences the catalytic activity of the catalysts towards ethanol oxidation. It is found that both catalysts show superior catalytic activity towards ethanol electrooxidation compared to pure Pt/C. However, PtCu/C displayed a better activity with respect to Pt(Cu)/C in terms of oxidation current and onset potential.

1. Introduction

In recent decades, low temperature fuel cells, such as direct ethanol fuel cells (DEFCs), have attracted much attention as alternative power sources for portable electronic devices due to their unique properties including low operating temperature, ease of liquid fuel handling, high energy density of the fuel ethanol (8 kWh kg^{-1}) as well as its low toxicity with respect to other fuels such as methanol [1–4].

Although DEFCs are good alternative power sources, their performance needs to be improved in order to make them suitable for many applications [5–7]. Carbon supported platinum (Pt) is commonly employed as anode catalyst for ethanol oxidation in low temperature fuel cells [8,9]. However, Pt is well known to be easily poisoned on its surface by adsorbed species such as carbon monoxide (CO), that are formed by the initial dehydrogenation of the alcohol molecules, hence leading to substantial losses in operation potentials [10,11]. To overcome this problem and improve the catalytic efficiency towards ethanol oxidation one possibility is to add a second metal to Pt to form Pt alloys or Pt core–shell catalysts. For ethanol electrooxidation, PtRu alloys are prominent catalysts with a reduced sensitivity towards CO poisoning compared to pure Pt [12,13]. Although the mechanisms for the enhanced activity with PtRu catalysts for ethanol oxidation are not yet fully understood, several studies suggest that is generally due to the ability of the promoter metal Ru to generate the oxygenated species necessary

* Corresponding author. Tel.: +1 905 721 8668x2936; fax: +1 905 721 3304.
E-mail addresses: m78ammam@yahoo.fr (M. Ammam), Brad.Easton@uoit.ca (E.B. Easton).

0378-7753/$ – see front matter © 2012 Elsevier B.V. All rights reserved.
http://dx.doi.org/10.1016/j.jpowsour.2012.07.143

for the complete oxidation of the alcohol at lower potentials [12–14]. On the other hand, removal of poisoning species adsorbed onto the catalyst surface has also been pointed out to be part of the mechanism [12–14].

A number of other low cost metal such as Co and Sn have also been combined with Pt to form low cost PtCo [15] and PtSn [16] alloy catalysts with improved catalytic properties towards ethanol oxidation. For Pt–Cu, although combination of Pt with Cu to form PtCu alloys or core shells catalysts have been intensively investigated for the oxygen reduction reaction (ORR) because of the superior activity of PtCu towards the ORR compared to Pt [17–21], only a handful of studies have been reported for alcohol oxidation using PtCu and this deals more specifically with methanol oxidation applications [22–24], rather than with ethanol electrooxidation.

We have recently reported the synthesis, characterization and the catalytic activity of binary PtMn/C [25], ternary PtMnX/C (X = Fe, Co, Ni, Cu, Mo and, Sn) [26], and quaternary PtMnCuX/C (X = Fe, Co, Ni, and Sn) and PtMnMoX/C (X = Fe, Co, Ni, Cu and Sn) [27] alloy catalysts and it was found that most of them show enhanced catalytic activity towards ethanol oxidation. The latter might be due in part to the synthetic method. In the course of this study, two catalysts PtCu/C alloy and Pt(Cu)/C attempted as core shells Cu covered by Pt were synthetized by the $NaBH_4$ method. The samples have been characterized by ICP, TEM, TGA, XRD, XPS, and cyclic voltammetry. Their catalytic activities towards ethanol oxidation were determined and compared with respect to pure Pt/C.

2. Experimental

2.1. Catalyst synthesis

PtCu/C was synthesized via the following route: $H_2PtCl_6 \cdot 6H_2O$ (Aldrich) and $CuCl_2 \cdot 2H_2O$ (Sigma–Aldrich) at the molar ratio of (11:89) are dissolved in ultrapure water (milliQ, 18.2 MΩcm). This molar ratio was chosen because our previous report for the synthesis of PtMn/C showed that even at low ratio of (10:90), the PtMn/C sample displayed high activity towards ethanol oxidation [25]. After 15 min of constant stirring Vulcan XC72R carbon black (Cabot) was added to the solution in an amount to give a total metal content of 20 wt%. PtCu nanoparticles supported on carbon were formed by reduction of the metal precursors with $NaBH_4$, which was added as a solid to the mixture in a weight ratio of 3:1 to metals. The resulting mixture was then left under constant stirring over night and the formed supported catalysts were collected via suction filtration, washed thoroughly with ultrapure water, ethanol, and acetone and finally dried over night at 80 °C.

Pt(Cu)/C was synthetized as follows: Cu/C nanoparticles were first synthetized by similar procedure as reported above for PtCu/C. Briefly, $CuCl_2 \cdot 2H_2O$ (Sigma–Aldrich) was dissolved in ultrapure water. After 15 min of constant stirring Vulcan XC72R carbon black (Cabot) was added to the solution in an amount to give a 17.8 wt%. total metal content. Cu nanoparticles supported on carbon were formed by reduction of the metal precursor with $NaBH_4$ which was added as a solid to the mixture in a weight ratio of 3:1 to metal. The resulting mixture was then left under constant stirring over night and the formed supported catalyst was collected via suction filtration, washed thoroughly with ultrapure water, ethanol, and acetone and finally dried over night at 80 °C. Afterwards, the synthesized Cu/C and $H_2PtCl_6 \cdot 6H_2O$ (Aldrich) were dissolved in ultrapure water at total molar ratio of 11:89 for Pt:Cu. After 15 min of constant stirring, the mixture was treated with $NaBH_4$ which was added as a solid in a weight ratio of 3:1 to metals and left under stirring over night and the formed Pt(Cu) supported on carbon was collected via suction filtration, washed thoroughly with ultrapure water, ethanol, and acetone and finally dried over night at 80 °C.

2.2. Materials characterization

Inductively Coupled Plasma Optical Emission Spectrometry (ICP-OES) was utilized for quantitative determination of metal content in the catalysts. 5 mg of each catalyst was dissolved in nitric acid (>70%) and left to dissolve for at least 1 week. Afterwards, the solutions were filtered off to separate the supporting carbon from the solution and yield a clear solution for ICP-OES analyses. Standardization was performed with three Pt and Cu solutions ranging from approximately 1–20 ppm. These standards contained approximately 2% nitric acid to ensure the complete dissolution and keep both sample and standard matrices equivalent.

Transmission Electron Microscopy (TEM) images were acquired using a Philips CM 10 instrument equipped with an AMT digital camera system. PtCu/C and Pt(Cu)/C powders were dissolved in ultrapure water and applied to nickel 400 mesh formvar coated carbon reinforced grids and allowed to dry under air. Grids were then scanned in a Philips CM 10 TEM at 100 kV.

Thermogravimetric analysis (TGA) of the catalysts was conducted using a TA Instruments Q600 SDT thermal analyzer. Samples were heated at a rate of 20 °C min^{-1} under air at (50 mL min^{-1}).

Power X-ray diffraction (XRD) patterns were obtained using Bruker D8 Advance powder X-ray diffractometer, with germanium monochrometer, Cu $K_{\alpha 1}$ radiation. The average grain size was determined from the broadening of the Pt(111) and Cu(111) peaks using the Scherrer equation.

X-ray photoelectron spectroscopy (XPS) was carried out by Thermo Instruments 310-F Microlab with a monochromatic Mg K_α X-ray source. The PtCu/C and Pt(Cu)/C samples were dispersed in a mixture of ethanol and ultrapure water (50:50), deposited on silicon wafer supports and oven dried then analyzed Thermo Instruments 310-F Microlab.

2.3. Electrochemical characterization

The electrocatalytic activity of the catalysts towards ethanol oxidation was measured through the preparation of electrode inks, which were prepared as follows: 11 mg of the synthesized electrocatalyst was dispersed in 500 μL of a mixture of ultrapure water and 2-propanol (1:1 by volume) and the suspension was stirred in an ultrasonic bath for 15 min. A total of 5 μL of the catalysts ink was immobilized onto the surface of a glassy carbon (GC) electrode (diam.=3 mm, CH Instruments) and dried at 80 °C for 20 min. Prior to use, the GC electrodes were first polished with 6, 3, and 1 μm alumina, then abundantly rinsed with ultrapure water and acetone. The final loading of metal catalysts on each electrode was 0.30 ± 0.03 mg cm^{-2}.

All electrochemical measurements were performed using a Solartron SI 1286 potentiostat controlled using Corrware software (Scribner Associates). A three-compartment electrochemical cell was used. The side arms contained an Ag/AgCl reference electrode and a platinum counter electrode. Measurements were made at room temperature using either N_2-purged 0.5 M H_2SO_4 (aq) or N_2-purged 0.5 M H_2SO_4 containing 0.17 M ethanol.

3. Results and discussion

3.1. Materials characterization

3.1.1. ICP-OES analyses

The calculated molar ratios used for the synthesis of the electrocatalysts and the atomic ratios determined by ICP-OES as well as the average grain size for each catalyst are compiled in Table 1. It can clearly be seen that compared to the calculated molar ratios used during the synthesis (11:89) for Pt and Cu respectively, the

Table 1
Calculated molar ratios and measured atomic ratios using ICP of the synthesized Pt/C, Cu/C, PtCu/C, and Pt(Cu)/C without and with including carbon. Also is shown the average grain size calculated from X-ray diffraction data using the Debye–Scherrer equation.

Electrocatalyst	Molar ratios used for the synthesis (metal only)			Molar ratios measured by ICP (metal only)			Grain size (nm±0.5)
	Pt	Cu	C	Pt	Cu	C	
Pt/C	100	0	–	100	0	–	8.5
Cu/C	–	100	–	–	100	–	37.3
PtCu/C	11	89	–	37	63	–	4.0
Pt(Cu)/C	11	89	–	38	62	–	3.0
Electrocatalyst	Total wt% used for the synthesis (metal + carbon)			Total wt% measured by ICP (metal + carbon)			Grain size (nm ± 0.5)
	Pt	Cu	C	Pt	Cu	C	
Pt/C	20.0	0.0	80.0	14.1	0.0	85.9	8.5
Cu/C	–	17.8	82.2	–	14.4	85.6	37.3
PtCu/C	2.2	17.8	80.0	4.0	6.8	89.2	4.0
Pt(Cu)/C	2.2	17.8	80.0	6.6	10.9	82.5	3.0

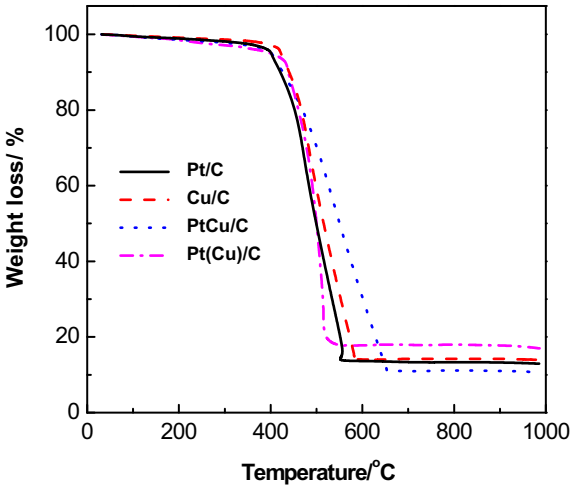

Fig. 2. TGA of the synthetized Pt/C, Cu/C, PtCu/C, and Pt(Cu)/C.

determined molar ratio of Pt seems to be higher and inversely the ratio of Cu decreased. This was not expected because energetically speaking; it is easier to reduce Cu than Pt [28]. Although at this stage, the reasons are not fully understood, it may have to do with the large ratio of the employed Cu^{2+} compared to Pt^{+4}. As a consequence, all Pt^{+4} was probably reduced, but some of the Cu^{2+} did not and still in the form of cations. On the other hand, the amount of the employed reducing agent $NaBH_4$ at the ratio of 3:1 to metals may also account. It is possible that 3 folds excess might not be enough to carry out the entire reduction process of the metal cations.

Table 1 also depicts that the ratio of the metal to carbon is higher for Pt(Cu)/C compared to PtCu/C. The latter may have to do with the

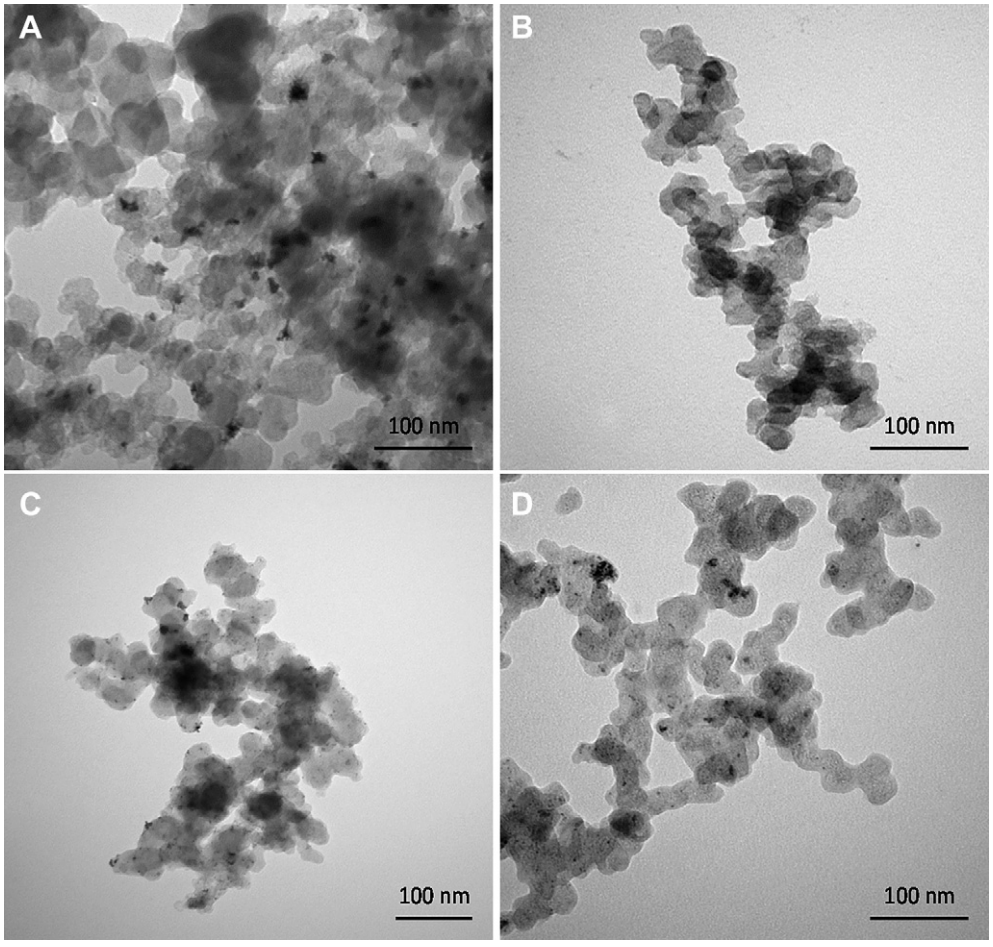

Fig. 1. TEM images of Pt/C (A), Cu/C (B), PtCu/C (C), and Pt(Cu)/C (D).

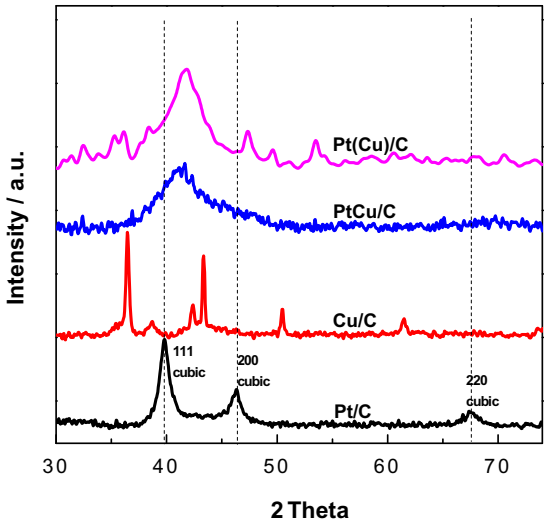

Fig. 3. X-ray diffractograms of the synthesized Pt/C, Cu/C, PtCu/C, and Pt(Cu)/C catalysts.

two distinctive synthetic steps used to produce Pt(Cu)/C. During the first step, high amount of Cu nanoparticles supported on carbon is formed because Cu^{+2} is quite easy to reduce using 3 folds excess $NaBH_4$ reducing agent. During the second step, Pt^{4+} and eventually some dissolved Cu from the Cu/C nanoparticles were reduced in presence of an additional 3 folds excess $NaBH_4$ to cover the remaining Cu/C nanoparticles with thin layers of Pt, Cu, or PtCu. As a result, by doubling the amount of $NaBH_4$ in the two step synthesis of Pt(Cu)/C, high ratio metal to carbon have been formed in Pt(Cu)/C compared to PtCu/C, where half the amount of $NaBH_4$ was used.

Table 1 also reveals similar grain size of PtCu/C (4 nm) and Pt(Cu)/C (3 nm) and surprisingly much larger grain size of Cu/C (37.3 nm). Since Pt(Cu)/C was synthesized by treating the Cu/C nanoparticles with $H_2PtCl_6 \cdot 6H_2O$ and $NaBH_4$, one may suggest that during this treatment Cu/C dissolves to yield smaller nanoparticles. The reason for that has probably to do with the large difference in potential between Cu and Pt which would form Pt–Cu galvanic couple, where Cu is the anodic pole and Pt is the cathodic pole. Mixture of Cu/C nanoparticles with Pt^{+4}, an oxidizing agent, will lead to corrosion of the Cu/C nanoparticles and, hence their dissolution. This may occur during the 15 min of the constant stirring of the mixture of Cu/C with $H_2PtCl_6 \cdot 6H_2O$. Upon addition of the reducing agent $NaBH_4$, Pt, and Cu cations will reduce and deposit essentially of the remaining smaller Cu/C nanoparticles to form Pt(Cu)/C.

3.1.2. TEM

The difference in grain size between Cu/C and Pt(Cu)/C can also be clearly seen in Fig. 1. While Cu/C shows large grain size and agglomerations, Pt(Cu)/C illustrates smaller grain sizes and better distribution on the carbon support. This confirms the results from XRD and the hypothesis of dissolution of Cu/C during its treatment with $H_2PtCl_6 \cdot 6H_2O$. Fig. 1 also depicts that PtCu/C and Pt(Cu)/C have similar morphologies in terms of grain size and distribution. However, Pt(Cu)/C display less agglomeration than PtCu/C. The latter may have to do with the two step synthesis of Pt(Cu)/C. The dissolution of Cu and deposition of PtCu and on the remaining Cu/C nanoparticles probably prevent agglomerations.

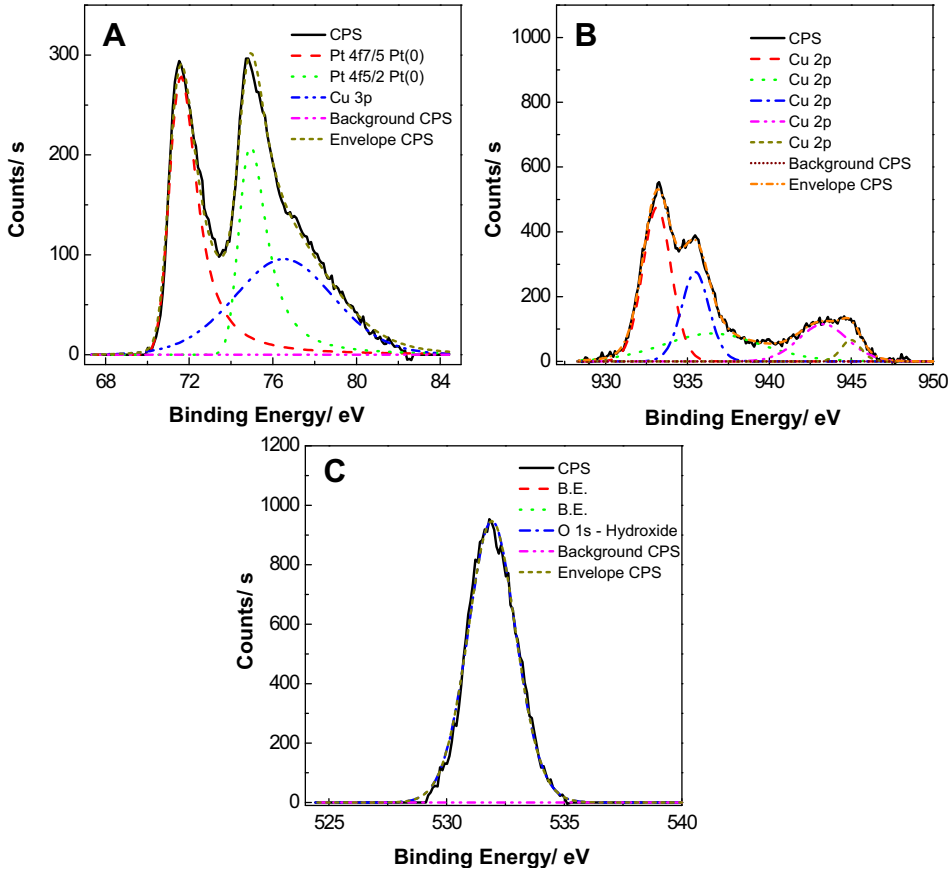

Fig. 4. XPS data of PtCu/C: Pt-4*f* and Cu-3P (A), Cu-2*p* (B), and O-1*s* (C).

3.1.3. TGA analysis

In order to verify the amount of the total metal fixed on the carbon support, the synthesized samples were analyzed by TGA and the results are shown in Fig. 2. It can be seen that Pt/C and Cu/C show similar amounts of the metal supported on carbon with 13.8% and 14.2%, respectively. By contrast, PtCu/C shows lower total metal percent (11.05%) and Pt(Cu)/C illustrates the highest total metal percent (18.1%). These results are very consistent with the results of ICP. Fig. 2 also depicts that PtCu/C and Pt(Cu)/C have different TGA profiles. While, Pt/C and Cu/C have close profiles of the catalytic combustion of carbon, the catalytic effect of PtCu/C towards the combustion of carbon seems to decrease compared to Pt(Cu)/C. This demonstrates that the composition and crystal structure of PtCu/C and Pt(Cu)/C are very different.

3.1.4. XRD analysis

The XRD patterns obtained for each electrocatalyst are illustrated in Fig. 3. Pt/C electrocatalyst displays three main Bragg peaks located at scattering angles of ca. 40°, 46°, and 67°, which are characteristic of the fcc structure of platinum [28]. Cu/C displays six main peaks located at scattering angles of ca. 36°, 38°, 42°, 43°, 50°, 61°, and 74°. The peaks located at 43°, 50°, and 74° correspond to the fcc of Cu [29]. The other peaks are related to presence of Cu-oxides, specifically CuO (36°, 38°) and Cu_2O (42°, 61°) [30]. The diffractograms of PtCu/C and Pt(Cu)/C clearly show the presence of the main Pt peaks, especially the (111) reflection located at 40° in pure Pt/C. However, the peaks look broader and display a shift towards higher angles. The broadening of the peaks can be related to the slight decrease in the grain size of PtCu/C and Pt(Cu)/C compared to Pt/C (Table 1). The slight shift towards higher angles may have to do with the difference in size between Pt and the co-catalyst Cu. In other words, Cu atoms are smaller than Pt and when replacing some Pt atoms in the lattice, unit cell become smaller, leading consequently to a decrease in d-spacing. On the other hand, while no Cu peaks can be observed in the diffractogram of PtCu/C, demonstrating incorporation of Cu into the Pt lattice to form intermetallic phases or alloy PtCu/C, low intensity Cu peaks can be observed in Pt(Cu)/C. The latter may suggest that the Cu/C nanoparticles were not entirely covered during their treatment with $H_2PtCl_6 \cdot 6H_2O$ in presence of $NaBH_4$. However, it is possible that some areas of the Cu/C nanoparticles remain unmodified. Also, Fig. 3 reveals the presence of other low intensity peaks which might not be related either to Pt or Cu. The latter might be due to formation of other types of oxides.

3.1.5. XPS characterization

In order to get a better idea on the composition as well as on the surface segregation of the synthesized PtCu/C and Pt(Cu)/C nanoparticles, the catalysts were analyzed by XPS and the results are shown in Figs. 4 and 5. XPS analysis of both catalysts PtCu/C and Pt(Cu)/C reveals the presence of Pt, Cu, and O in their surface compositions. This suggests that no Pt/C or Cu/C separate nanoparticles were formed in both catalysts. Also, it can be noticed that PtCu/C show high amount of Pt and low amount of Cu and O. By contrast, Pt(Cu)/C reveals high amount of copper and oxygen and low amount of platinum. The latter suggest that PtCu/C is Pt rich at

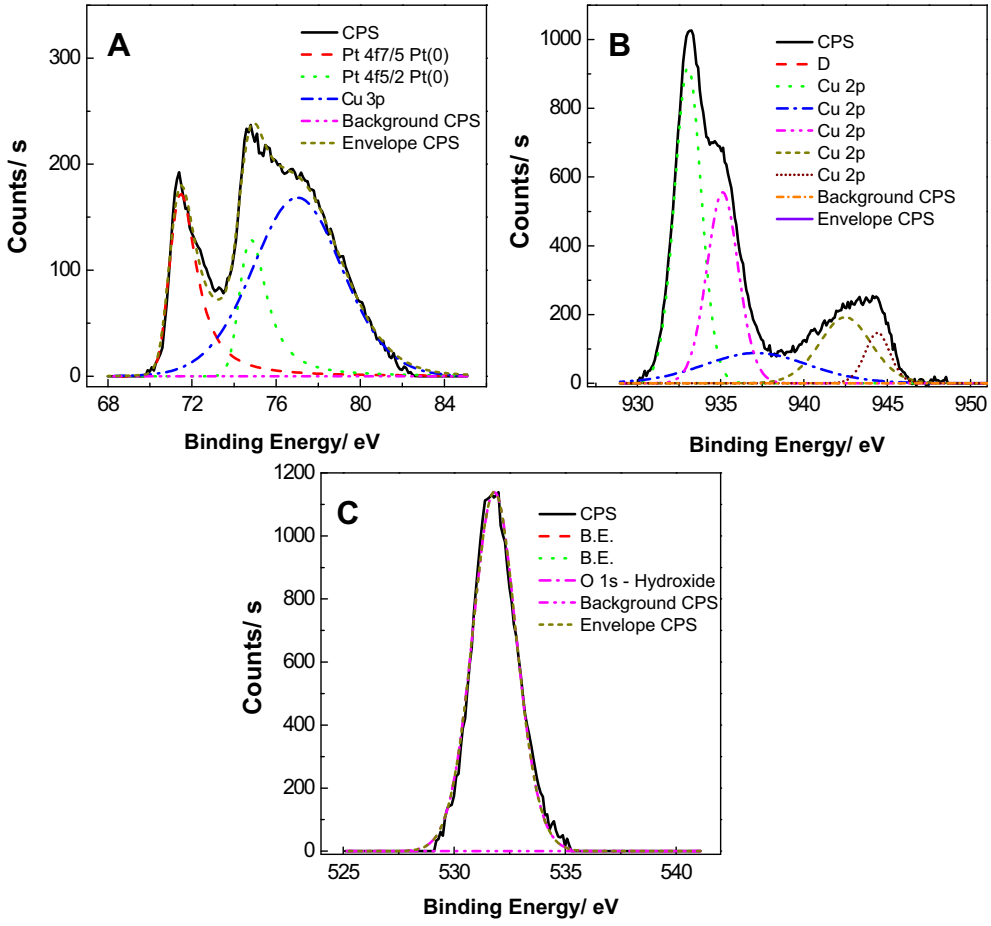

Fig. 5. XPS data of Pt(Cu)/C: Pt-4f and Cu-3P (A), Cu-2*p* (B), and O-1*s* (C).

the surface of the nanoparticle, whereas Pt(Cu)/C is Cu rich at the surface of the nanoparticles.

3.1.6. Cyclic voltammetry

The cyclic voltammetry curves of Pt/C, Cu/C, PtCu/C, and Pt(Cu)/C are shown in Fig. 6. The cyclic voltammetry curve of Pt/C is characterized by two regions commonly identified as the oxide region in the positive potential and hydrogen adsorption region at the negative potentials. The cyclic voltammetry curve of Cu/C displays a very different pattern from the one observed for Pt. Several redox waves related to the oxidation and reduction of the Cu/C centers, with passage from Cu^0 to Cu^{II} can be observed [31]. Fig. 6C and D depicts that the cyclic voltammetry curves of PtCu/C and Pt(Cu)/C are much more close to the cyclic voltammetry curve of Pt/C, rather than Cu/C. Also, changes in the oxide as well as in the hydrogen region can be noticed in the curves of PtCu/C and Pt(Cu)/C with respect to Pt/C. This suggest that Cu was incorporated in the Pt lattice to form alloy catalysts PtCu/C and Pt(Cu)/C. The decrease in the charge of the oxide and hydrogen adsorption regions is attributed to the decrease in the Pt content in PtCu/C and Pt(Cu)/C compared to Pt/C. Fig. 6B and C also reveals a slight decrease in the current response in both oxide and hydrogen adsorption regions after 200 cycles. The decrease recorded for Pt(Cu)/C is more significant compared to PtCu/C. The latter indicate minimal corrosion rate of the PtCu/C and Pt(Cu)/C in sulfuric acid despite of their high content in Cu. Furthermore, PtCu/C seems to be more stable than Pt(Cu)/C. This may be related to surface segregation of the nanoparticles, which as previously demonstrated by XPS are Pt rich for PtCu/C and Cu rich for Pt(Cu)/C catalyst.

4. Catalytic oxidation towards ethanol

Fig. 7A depicts a comparison of the cyclic voltammetry curves of Pt/C, PtCu/C, and Pt(Cu)/C in 0.5 M H_2SO_4 containing 0.17 M ethanol. No catalytic activity towards ethanol oxidation was observed with Cu/C (data not shown). Fig. 7A displays that compared to pure Pt/C, both samples PtCu/C and Pt(Cu)/C exhibit higher catalytic activity towards ethanol oxidation. The latter can be attributed first to the grain size of the formed nanoparticles, which are smaller and have better distribution on the supporting carbon for PtCu/C and Pt(Cu)/C with respect to Pt/C (Fig. 1). On the other hand, the composition of the catalyst may also have a strong influence on the catalytic activity of the catalyst towards ethanol oxidation [25–27]. Presence of Cu in the Pt lattice may promote a different oxidation mechanism by preventing, for example, formation of adsorbed species issued from the decomposition of ethanol. This may clearly be observed in the shape of the cyclic voltammograms of Fig. 7A. While for Pt an increase in the catalytic current is recorded during the reverse scan, revealing a catalytic process of adsorbed species on the surface of the Pt/C catalyst, both PtCu/C and Pt(Cu)/C display no increase in the current during the reverse scan, demonstrating that no electrocatalysis of adsorbed species on the catalyst surface took place. The latter is reflected in the average number of the electrons exchanged during the

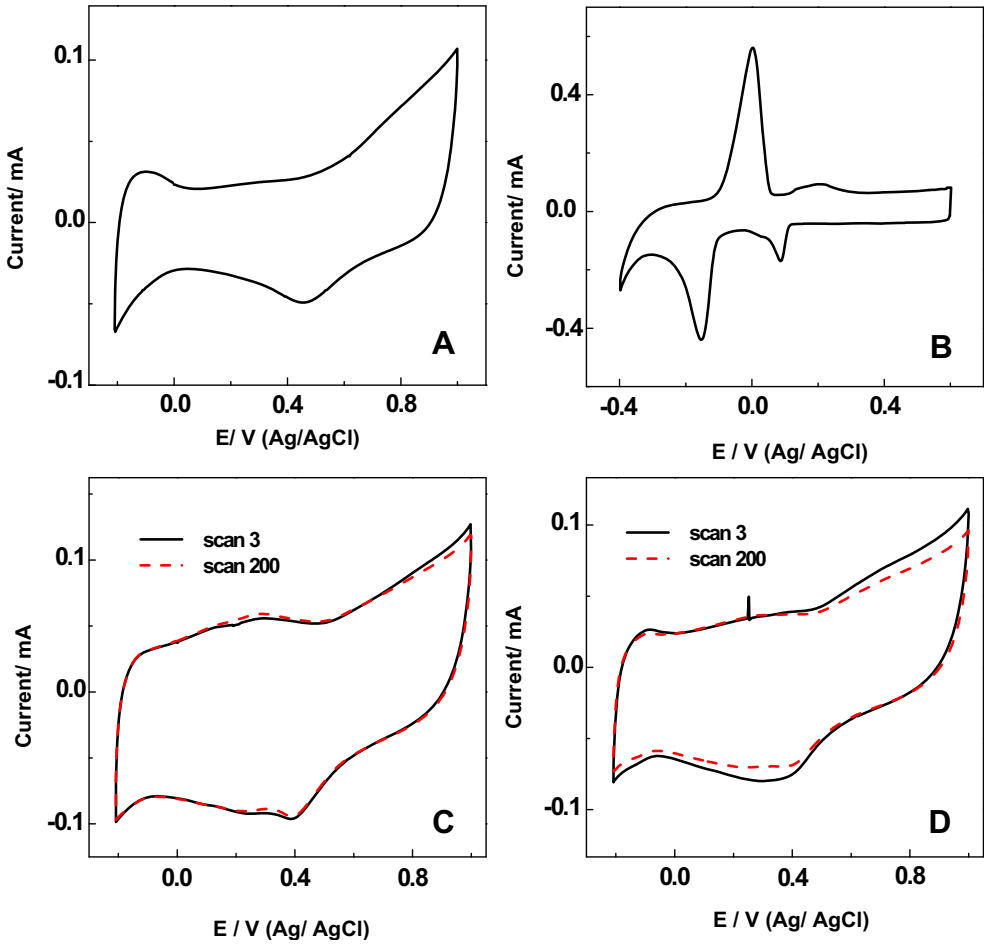

Fig. 6. Cyclic voltammetry curves of Pt/C (A), Cu/C (B), PtCu/C (C), and Pt(Cu)/C (D) catalysts in 0.5 M H_2SO_4.

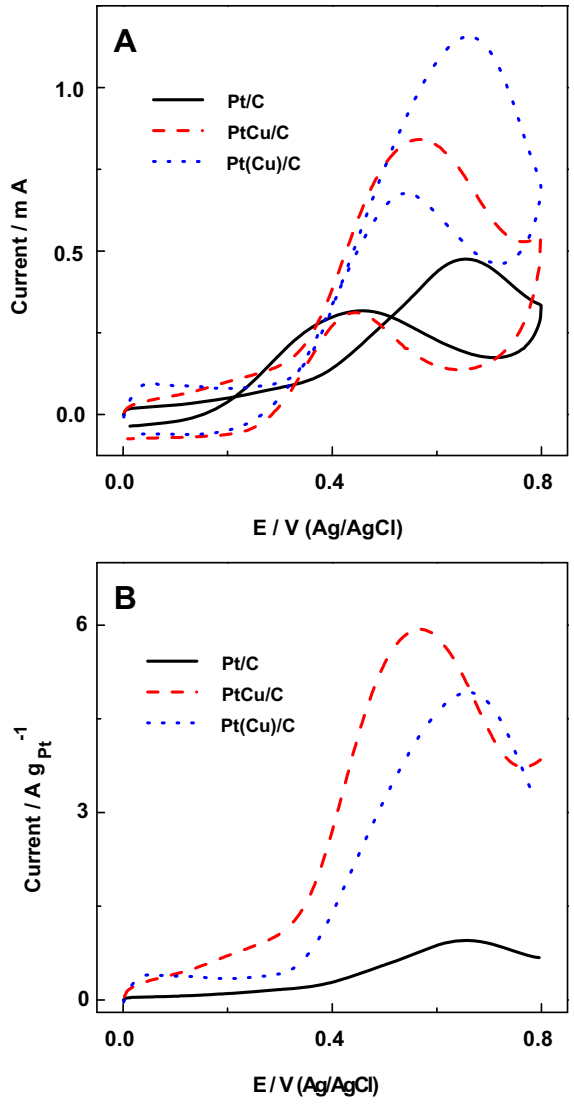

Fig. 7. (A) Cyclic voltammetry curves of Pt/C, PtCu/C, and Pt(Cu)/C electrocatalysts in 0.5 M H_2SO_4 containing 0.17 M ethanol, (B) normalized Fig. (A) per mg of Pt without the reverse scan. Scan rate: 20 mV s^{-1}.

oxidation process of ethanol estimated from peak current in the cyclic voltammograms, which is illustrated in Eq. (1) [32]:

$$n = 4RTI_p/FQv \quad (1)$$

where n is the number of the exchanged electrons, I_p is the peak current intensity, Q is the electrical charge, v is the scan rate and R, T, F have their usual meaning.

Since our measurement conditions are identical for all catalysts and neither catalysts has a substantially different electrochemically active surface area, we can infer that current gain must be due to the change in electrons transferred. The estimated average number of the electrons for ethanol oxidation under the same conditions are 5.32, 9.04 and 8.54 electrons for respectively Pt/C, PtCu/C and Pt(Cu)/C. This means that the process of CO_2 generation, which generates 12 electrons, is likely more favorable with PtCu/C and Pt(Cu)/C rather than with Pt/C catalyst. This is in agreement with the low rate of CO_2 genetration with Pt/C catalysts reported by Ghumman et al. [33] and hence, demostrates the superior catalytic activity of the binary PtCu/C and Pt(Cu)/C catalysts compared to Pt/C.

Table 2
Summary of the synthesized alloys Pt/C, PtCu/C, and Pt(Cu)/C and their normalized relative activities to pure Pt estimated at 0.45 V and 0.60 V vs. Ag/AgCl. Also is shown the onset potential of ethanol oxidation for each catalyst.

Synthesized catalyst	Relative activity to pure Pt		Onset potential (V)
	0.45 V	0.60 V	
Pt/C	1	1	0.328
PtCu/C	12.9	7.1	0.265
Pt(Cu)/C	6.9	5.7	0.297

Fig. 7B compares ethanol oxidation activity normalized to the amount of Pt as well as total metal content in the catalyst estimated by TGA. The normalized relative activities towards ethanol oxidation of the synthesized catalysts PtCu/C and Pt(Cu)/C per gram of Pt estimated at 0.45 V and 0.60 V are listed in Table 2. It can be seen that the catalytic activity estimated at low potential of 0.45 V are about 12.9 and 6.9 folds higher for PtCu/C and Pt(Cu)/C, respectively. At high polarization potential of 0.6 V, there is a decrease in the relative activities to about 7.1 and 5.7 for PtCu/C and Pt(Cu)/C,

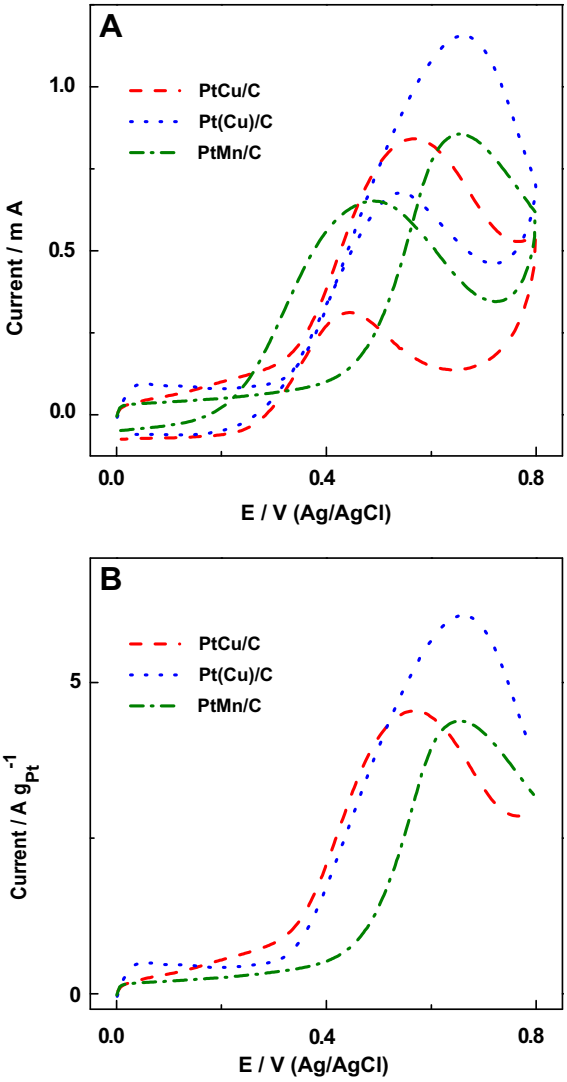

Fig. 8. (A) Comparison between the cyclic voltammetry curves of PtCu/C and Pt(Cu)/C with the previously reported PtMn (39:61)/C in 0.5 M H_2SO_4 containing 0.17 M ethanol, (B) normalized Fig. (A) per mg of Pt without the reverse scan. Scan rate: 20 mV s^{-1}.

respectively. This suggest that Pt/C performs better at higher polarizations potentials, while PtCu/C and Pt(Cu)/C seem to perform better at lower polarization potentials. The latter is further confirmed in the estimated onset potentials of ethanol oxidation displayed in Table 2. It can be observed that compared to Pt/C, the onset potential of ethanol oxidation is shifted towards less positive values with PtCu/C and Pt(Cu)/C. Precisely, 63 mV and 31 mV are respectively the gains in potential recorded with PtCu/C and Pt(Cu)/C. This means that ethanol oxidation is facilitated and needs less overpotential with the catalysts PtCu/C and Pt(Cu)/C. Fig. 7 and Table 2 also reveal that PtCu/C has better catalytic activity towards ethanol oxidation in terms of normalized current and onset potential. The latter might be related to surface segregation of each catalyst PtCu/C and Pt(Cu)/C. Although the ratio of Pt to Cu determined by ICP are similar for PtCu/C and Pt(Cu)/C (Table 1), XPS revealed that PtCu/C is Pt rich at the surface. By contrast, Pt(Cu)/C is Cu rich at the surface of the nanoparticles.

It can be difficult to compare activities of the synthesized PtCu/C and Pt(Cu)/C with other reported binary alloys catalysts in the literature due to differences in experimental conditions. However, the activity of PtCu/C and Pt(Cu)/C in this work is compared to our previously reported activity for PtMn/C tested under identical conditions [25], which is shown in Fig. 8. Fig. 8B clearly depicts more than 100 mV gain in potential for PtCu/C and Pt(Cu)/C compared to PtMn/C. Also the current intensity of Pt(Cu)/C is higher than PtMn/C. This means that ethanol oxidation is energetically more favorable with PtCu/C and Pt(Cu)/C compared to PtMn/C.

5. Stability

The superior performance of PtCu/C and Pt(Cu)/C samples towards ethanol oxidation are also observed by chronoamperometry (Fig. 9A). In all current–time curves there is an initial current drop during the first 400 s where Pt(Cu)/C display slightly higher current intensities with respect to PtCu/C. Afterwards, PtCu/C continuous with a slower decay compared to Pt(Cu)/C and its current intensities becomes higher than those recorded with Pt(Cu)/C after about 1000 s. This demonstrates the relative stability of PtCu/C compared to Pt(Cu)/C in the sulfuric acid media containing ethanol. This is further confirmed by Figs. 9B and 8C which illustrate respectively the cyclic voltammetry curve of PtCu/C and Pt(Cu)/C in 0.5 M H_2SO_4 containing a higher concentration of ethanol (1 M) after 2 and 200 cycles. As expected, the decrease in the current after 200 cycles in more significant for Pt(Cu)/C than for PtCu/C. Surface segregation determined by XPS may be the reason. The richness of Pt(Cu)/C with Cu at the surface of the nanoparticles may accelerate the corrosion process of the nanoparticles compared to PtCu/C where the nanoparticles are Pt rich [34], thus leading to less stability. On the other hand, contrary to the behavior of PtCu/C and Pt(Cu)/C in 0.17 M ethanol, where the shape of the cyclic voltammograms are different from that of Pt/C (Fig. 7), at 1 M ethanol, Fig. 9B and C depict similar trends of PtCu/C and Pt(Cu)/C with respect to Pt/C (Fig. 7A). The reason for that may have to do with the ethanol concentration. Because the concentration is high in Fig. 9B and C (1 M), the reaction products generated at the

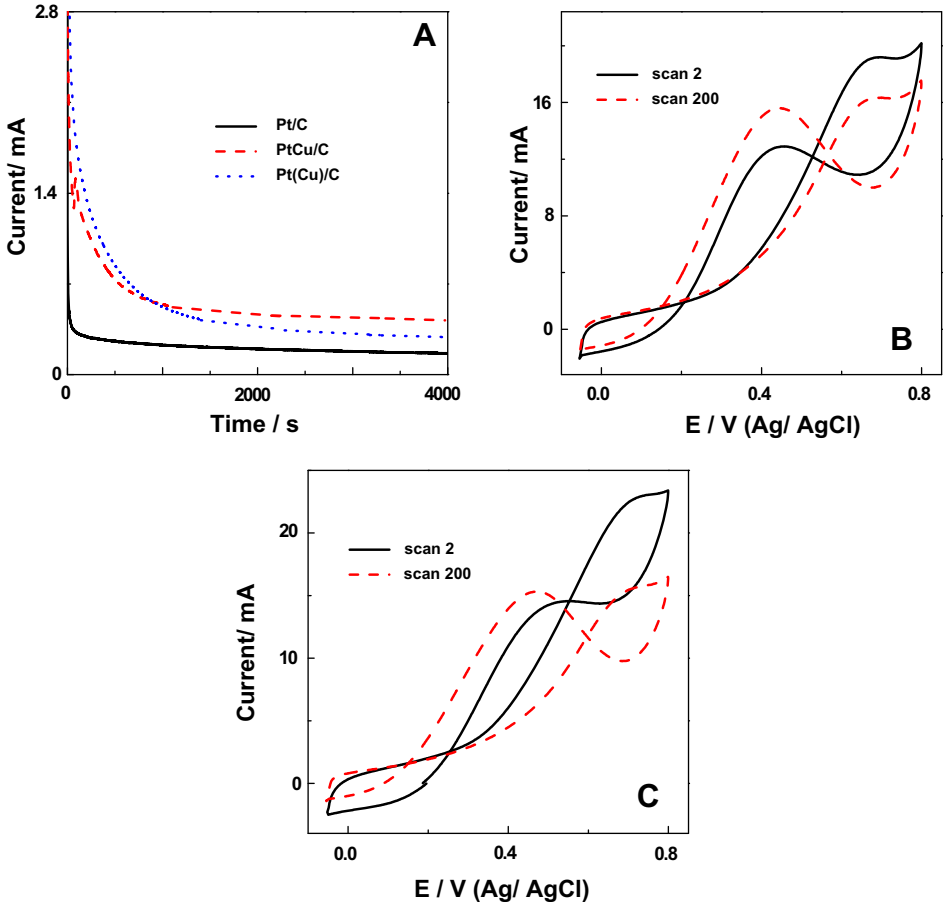

Fig. 9. (A) Chronoamperometry curves at+0.65 V in 0.5 M H_2SO_4 containing 0.17 M ethanol of Pt/C, PtCu/C, and Pt(Cu)/C catalysts. (B) and (C) are cyclic voltammetry curves of, respectively, PtCu/C and Pt(Cu)/C catalysts in 0.5 M H_2SO_4 containing 1 M ethanol after 2 and 200 cycles at a scan rate of 50 mV s^{-1}.

electrode are also significant. As a consequent, the amount of the adsorbed species increased, leading to a different mechanism.

6. Conclusions

In this account, binary catalysts containing Pt and Cu have been synthetized by two different methods. The first method consists of mixing Pt^{4+} and Cu^{2+} cations in presence of $NaBH_4$ to form PtCu/C alloy catalyst. In the second method, Cu/C nanoparticles were first synthetized then treated with Pt^{+4} in presence of $NaBH_4$ in an attempt to form core shells Cu covered by Pt, Pt(Cu)/C. The synthesized catalysts PtCu/C and Pt(Cu)/C were characterized by Inductively Plasma Emission Spectroscopy (ICP), Transmission Electron Microscopy (TEM), Thermogravimetric Analysis (TGA), X-ray diffraction (XRD), X-ray Photoelectron Spectroscopy (XPS) and Electrochemistry. XRD studies indicate that Pt–Cu alloy has formed in both cases even using the second synthetic method that is supposed to yield Cu covered by Pt core shells. The latter was attributed to the dissolution of Cu/C nanoparticles during their treatment with Pt^{4+}. This was confirmed by XRD and TEM where significant decrease in the grain size from ~37.2 nm obtained for Cu/C to ~3 nm for Pt(Cu)/C was observed. While ICP analysis revealed similar Pt and Cu contents in each catalyst, XPS showed that PtCu/C is Pt rich at the surface and Pt(Cu)/C is Cu rich at the surface of the nanoparticles. In turn, this surface segregation influences the catalytic activity of the catalysts towards ethanol oxidation. It is found that both catalysts show superior catalytic activity towards ethanol electrooxidation compared to pure Pt/C. However, PtCu/C displayed a better activity with respect to Pt(Cu)/C in terms of oxidation current and onset potential. Future work will focus on the detailed study of the reaction products generated from the ethanol oxidation using techniques such as in situ infrared reflection-absorption spectroscopy as well as the direct application of these catalysts in fuel cell prototype.

Acknowledgement

This work was supported by Alcohol Countermeasure Systems Corp., the Natural Sciences and Engineering Research Council (NSERC) of Canada and UOIT. We thank Wen He Gong (McMaster University) for the XRD data, Michael Allison (UOIT) for assistance with the ICP measurements, Dr Richard B. Gardiner (University of Western Ontario) for the TEM images and Mark C. Biesinger (University of Western Ontario) for XPS data.

References

[1] J.M. Feliu, M. Herrero, in: W. Vielstich, A. Lamm, H.A. Gasteiger (Eds.), Handbook of Fuel Cells, Wiley & Sons, Ltd., Chichester, 2003 (Chapter 42).
[2] A.S. Arico, S. Srinivasan, V. Antonucci, Fuel Cells 1 (2001) 133.
[3] K. Kordesch, G. Simader, Fuel Cells and Their Applications, VCH, Weinheim, 1996.
[4] E.V. Spinace, R.R. Dias, M. Brandalise, M. Linardi, A.O. Neto, Ionics 16 (2010) 91.
[5] W. Qian, D.P. Wilkinson, J. Shen, H. Wang, J. Zhang, Journal of Power Sources 154 (2006) 202.
[6] S.Y. Shen, T.S. Zhao, J.B. Xu, Y.S. Li, Journal of Power Sources 195 (2010) 1001.
[7] S. Song, P. Tsiakaras, Applied Catalysis B: Environmental 63 (2006) 187.
[8] C. Xu, L. Cheng, P. Shen, Y. Liu, Electrochemistry Communications 9 (2007) 997.
[9] Z.Y. Zhou, Z.Z. Huang, D.J. Chen, Q. Wang, N. Tian, S.G. Sun, Angewandte Chemie International Edition 49 (2010) 411.
[10] S.C. Hall, V. Subramanian, G. Teeter, B. Rambabau, Solid State Ionics 175 (2004) 809.
[11] F. Vigier, C. Coutanceau, F. Hahn, E.M. Belgsir, C. Lamy, Journal of Electroanalytical Chemistry 563 (2004) 81.
[12] H. Wang, Z. Jusys, R.J. Behm, Journal of Power Sources 154 (2006) 351.
[13] F. Colmati, E. Antolini, E.R. Gonzalez, Journal of Power Sources 157 (2006) 98.
[14] N. Fujiwara, K.A. Friedrich, U. Stimming, Journal of Electroanalytical Chemistry 472 (1999) 120.
[15] T. Lopes, E. Antolini, F. Colmati, E.R. Gonzalez, Journal of Power Sources 164 (2007) 111.
[16] L. Jiang, G. Sun, S. Sun, J. Liu, S. Tang, H. Li, B. Zhou, Q. Xin, Electrochimica Acta 50 (2005) 5384.
[17] R. Srivastava, P. Mani, N. Hahn, P. Strasser, Angewandte Chemie International Edition 46 (2007) 8988.
[18] S. Koh, N. Halm, P. Strasser, ECS Transactions 3 (2006) 139.
[19] M. Oezaslan, F. Hasche, P. Strasser, Journal of The Electrochemical Society 159 (2010) B444.
[20] K. Jayasayee1, J.A. Rob Van Veen, T.G. Manivasagam, S. Celebi, E.J.M. Hensen, F.A. de Bruijn, Applied Catalysis B: Environmental 111–112 (2012) 515.
[21] M. Oezaslan, P. Strasser, Journal of Power Sources 196 (2011) 5240.
[22] T. Page, R. Johnson, J. Hormes, S. Noding, B. Rambabu, Journal of Electroanalytical Chemistry 485 (2000) 34.
[23] H. Yang, L. Dai, D. Xu, J. Fang, S. Zou, Electrochimica Acta 55 (2010) 8000.
[24] D. Xu, Z. Liu, H. Yang, Q. Liu, J. Zhang, J. Fang, S. Zou, K. Sun, Angewandte Chemie International Edition 48 (2009) 4217.
[25] M. Ammam, L.E. Prest, A.D. Pauric, E.B. Easton, Journal of the Electrochemical Society 159 (2012) B195.
[26] M. Ammam, E.B. Easton, Journal of the Electrochemical Society 159 (2012) B635.
[27] M. Ammam, E.B. Easton, Journal of Power Sources 215 (2012) 188.
[28] G.C. Li, P.G. Pickup, Electrochimica Acta 52 (2006) 1033.
[29] W.H. Cheng, Applied Catalysis A: General 130 (1995) 13.
[30] Y. Li, Q. Fu, M.F. Stephanopoulos, Applied Catalysis B: Environmental 27 (2000) 179.
[31] T.H. Tsai, T.W. Chen, S.M. Chen, International Journal of Electrochemical Sciences 6 (2011) 4628.
[32] P. Somasundaran, Encylopedia of Surface and Colloid Science, Cyclic Voltammetry at Electrode Interface, Marcel Dekker, Inc., New York, 2004, p. 178 (updated supplement).
[33] A. Ghumman, C. Vink, O. Yepez, P.G. Pickup, Journal of Power Sources 177 (2008) 71–76.
[34] A. Marcu, G. Toth, R. Srivastava, P. Strasser, Journal of Power Sources 208 (2012) 288.